Adiabatic theory of strong-field photoelectron momentum distributions near a backward rescattering caustic

Toru Morishita[1] and Oleg I. Tolstikhin[2]

[1]*Institute for Advanced Science, The University of Electro-Communications, 1-5-1 Chofu-ga-oka, Chofu-shi, Tokyo 182-8585, Japan*

[2]*Moscow Institute of Physics and Technology, Dolgoprudny 141700, Russia*

(Received 17 September 2017; published 17 November 2017)

We present a comprehensive treatise on the derivation of the factorization formula describing strong-field photoelectron momentum distributions near the outermost backward rescattering caustic within the adiabatic theory and its validation by calculations. The formula derived holds for ionization by linearly polarized laser pulses of sufficiently low frequency and becomes exact as the frequency tends to zero for a fixed pulse amplitude. The convergence of the results obtained from the formula to accurate photoelectron momentum distributions obtained by solving the time-dependent Schrödinger equation is demonstrated. The formula is shown to work quantitatively in both tunneling and over-the-barrier regimes of ionization for finite-range potentials as well as potentials with a Coulomb tail. This paves the way for future applications of the present theory in strong-field physics. In particular, the explicit analytical form of the returning photoelectron wave packet given here enables one to extract differential cross sections for elastic scattering of a photoelectron on the parent ion from experimental photoelectron momentum distributions.

DOI: 10.1103/PhysRevA.96.053416

I. INTRODUCTION

Photoelectron momentum distributions (PEMDs) resulting from the ionization of atoms and molecules by intense low-frequency laser pulses contain valuable information about the electronic and nuclear structure of the target. The development of methods of extracting this information, potentially in a time-resolved manner, is one of the fundamental tasks of strong-field physics [1]. The different parts of a strong-field PEMD reflect different aspects of the ionization dynamics and encode different target structure information. Here, we focus on one particular feature specific to PEMDs generated by linearly polarized pulses and related to rescattering. The region of localization of such PEMDs in photoelectron momentum space in directions close to the polarization axis has a well-defined classical boundary determined by the coalescence of a pair of long and short trajectories originating from the same half-cycle of the laser field and undergoing one near-backward rescattering after the field changes sign [2]. Each half-cycle produces a pair of such trajectories; the surface in their final momentum space where the trajectories coalesce we call the backward rescattering caustic (BRC). The classical boundary of a PEMD is given by the outermost BRC. In directions closer to the normal to the polarization axis this BRC may enter the region where the contribution from direct electrons, which have not experienced rescattering, dominates. In this case, the boundary of the PEMD becomes more diffuse and its location is determined by properties of the initial quantum state. The feature we are interested in consists in the property of factorization of strong-field PEMDs in the vicinity of the outermost BRC into the differential cross section (DCS) for elastic scattering of a photoelectron on the parent ion and a returning photoelectron wave packet (RWP) [3]. This property lays the foundation for a method of extracting DCSs from experimental PEMDs, which has attracted much attention in recent years [4–25].

In the original paper [3], the factorization formula (FF) was inferred on physical grounds from the results of numerical calculations. The notion of RWP introduced there was defined by the FF itself; no explicit form of the RWP was given. Some additional arguments and calculations in support of the factorization presented in a followup paper [4] did not change the situation. At the same time, in order to extract a DCS, one obviously needs to know the RWP. Two approaches to resolving this issue exist in the literature.

One approach aims at obtaining an explicit form of the RWP by deriving the FF analytically. This was done for several models under different theoretical assumptions. In Ref. [5], the FF was derived heuristically (as stated in Ref. [6]) within the strong-field approximation. In Refs. [7,8], it was derived for a short-range potential treated using the effective range theory and then phenomenologically generalized (as stated in Ref. [9]) to realistic atomic potentials. In Ref. [10], it was derived for a one-dimensional zero-range potential model in the adiabatic approximation. The FF was shown to hold for sufficiently low frequency and high intensity of the laser field near the outermost BRC, where only one pair of coalescing rescattering trajectories contributes to the PEMD. Its validity was confirmed by comparison with accurate PEMDs obtained by solving the time-dependent Schrödinger equation (TDSE) [7–10]. These studies made an important contribution to the development of the method: they justified the conjecture of factorization [3] and uncovered the analytical structure of the RWP for the models considered. However, they did not affect the way how the method is currently used in applications.

In the majority of studies where the FF was actually used for extracting DCSs [11–17] and related target structure information such as charge density [18,19] and molecular bond lengths [20–24] from experimental PEMDs, another more pragmatic approach was adopted. In this approach, the need of an explicit form of the RWP is eliminated by making some plausible assumptions regarding its dependence on kinematic characteristics of the rescattering event. Thus, in Refs. [11–18] the extraction procedure was based on the following approximations: (a) the experimental information was extracted from

a sphere approximating the outermost BRC near the backward rescattering direction, (b) the incident momentum of rescattering at the sphere was assumed to be constant, and (c) the RWP was assumed to be independent of the scattering angle. These approximations indeed hold near the backward rescattering direction, but incur errors which grow as the scattering angle decreases. Anyway, under these approximations one can extract the dependence of a DCS on the scattering angle at a fixed incident momentum without knowing the RWP, but only up to an unknown incident-momentum-dependent factor. The extracted DCSs were shown to be in good agreement with the results of independent scattering calculations within the single-active-electron approximation [11–13,18] and using a configuration interaction approach [15–17], which was a success in demonstrating the potentiality of the method. In the absence of a firmly recognized relation between the origin of this success and the analytical justification of the FF, applications of the method were extended to situations where the formula does not hold. For example, in Refs. [19–24], in addition to the approximations listed above, the sphere from which the experimental information is extracted was chosen in an *ad hoc* way somewhere at intermediate photoelectron energies far from the outermost BRC. Although the results turned out to be consistent with scattering calculations performed for their analysis, in this case the extraction procedure lacks analytical support.

As far as we know, there is only one paper [25] where an analytically derived RWP was used for extracting DCSs from experimental PEMDs, and this was done as prescribed by the theory, without any additional approximations. In this paper, the method was developed in two directions. Experimentally, it was shown that the use of few-cycle pulses with carrier-envelope phase control provides access to the dependence of a DCS on the incident momentum, which is extremely difficult to achieve by other experimental techniques [17]. Theoretically, an analytical form of the RWP was derived from the adiabatic theory [26] and used in the extraction procedure. As a result, the DCS for elastic scattering of an electron on an ion of xenon was for the first time extracted up to a constant factor as a function of both the scattering angle and the incident momentum in a wide range of these variables. The scheme demonstrated in Ref. [25] is free from approximations and ambiguities of previous studies. This elevates the method to a quantitative level and opens new opportunities, e.g., may enable one to detect multielectron effects in DCS.

In this paper, we elaborate the theoretical part of the scheme, which is intended to pave the way for its future applications. We present a comprehensive treatment of all issues related to the derivation and validation of the FF within the adiabatic theory [26]. The paper is organized as follows. In Sec. II, we document the derivation of the FF, which was skipped in the previous short paper [25]. The resulting formula generalizes and corrects in several important ways the one reported earlier. In particular, the derivation reveals a quantum shift of the BRC as well as certain strong-field effects in the RWP which for simplicity were disregarded in Ref. [25]. In Sec. III, the analytical results are illustrated by calculations. We thoroughly compare the predictions of the FF with accurate PEMDs obtained by solving the TDSE for a number of target potentials and laser pulses. Section IV concludes the paper.

II. THEORY

A. Basic equations

We consider an atom or molecule treated in the single-active-electron and frozen-nuclei approximations interacting with a linearly polarized intense low-frequency laser pulse. The interaction of the active electron with the parent ion is described by the potential $V(\mathbf{r})$. To comply with the condition of applicability of the adiabatic theory [26], we assume that this potential vanishes sufficiently rapidly beyond a finite radius $r = a$. The argumentation and calculations presented below show that the adiabatic theory holds for describing near-backward rescattered electrons, which we focus on here, even if the potential has a Coulomb tail; however, to stay on solid mathematical grounds, in the derivation we assume it to have a finite range. The electric field of the laser pulse is represented by $\mathbf{F}(t) = F(t)\mathbf{e}_z$, where $F(\pm\infty) = 0$. The TDSE for the active electron in the dipole approximation and length gauge reads (atomic units are used throughout)

$$i\,\frac{\partial\psi(\mathbf{r},t)}{\partial t} = \left[-\frac{1}{2}\,\Delta + V(\mathbf{r}) + F(t)z\right]\psi(\mathbf{r},t). \tag{1}$$

We are interested in the solution satisfying the initial condition

$$\psi(\mathbf{r},t \to -\infty) = \phi_0(\mathbf{r})e^{-iE_0t}, \tag{2}$$

where $E_0 < 0$ and $\phi_0(\mathbf{r})$ are the energy and normalized wave function of a bound state of the unperturbed system

$$\left[-\tfrac{1}{2}\Delta + V(\mathbf{r}) - E_0\right]\phi_0(\mathbf{r}) = 0. \tag{3}$$

The observable to be discussed is the PEMD $P(\mathbf{k})$ defined by

$$P(\mathbf{k}) = |I(\mathbf{k})|^2, \quad P_{\rm ion} = \int P(\mathbf{k})\,\frac{d\mathbf{k}}{(2\pi)^3}, \tag{4}$$

where $I(\mathbf{k})$ is the ionization amplitude

$$I(\mathbf{k}) = e^{ik^2t/2}\int \varphi(\mathbf{r};-\mathbf{k})\psi(\mathbf{r},t)\,d\mathbf{r}\Big|_{t\to\infty}, \tag{5}$$

and $P_{\rm ion}$ is the total ionization probability. Here, $\varphi(\mathbf{r};\mathbf{k})$ is the scattering state of the unperturbed system with incident momentum $\mathbf{k}$,

$$\left[-\tfrac{1}{2}\Delta + V(\mathbf{r}) - \tfrac{1}{2}\mathbf{k}^2\right]\varphi(\mathbf{r};\mathbf{k}) = 0, \tag{6a}$$

$$\varphi(\mathbf{r};\mathbf{k})|_{r\to\infty} = e^{i\mathbf{kr}} + f(\mathbf{k},\Omega)\,\frac{e^{ikr}}{r}, \tag{6b}$$

where $f(\mathbf{k},\Omega)$ is the scattering amplitude and $\Omega = (\theta,\varphi)$ denotes scattering angles which in the present case it is convenient to choose as spherical angles defining the direction of $\mathbf{r}$ in a coordinate frame with the z axis pointing along $\mathbf{k}$. For atoms, the potential $V(\mathbf{r})$ is spherically symmetric and $f(\mathbf{k},\Omega)$ depends only on the absolute value k of the incident momentum and the angle θ between $\mathbf{k}$ and $\mathbf{r}$. For molecules, the potential reflects the shape of the internuclear configuration and its orientation with respect to the polarization axis and does not generally have any symmetry. In this case, $f(\mathbf{k},\Omega)$ depends on all five of its arguments. The DCS is given by $|f(\mathbf{k},\Omega)|^2$ [27].

B. Adiabatic theory

The adiabatic theory [26] amounts to the asymptotic solution of the problem for $\epsilon \to 0$, where ϵ is the adiabatic parameter giving the ratio of the target and laser field time scales. This parameter can be estimated as $\epsilon \sim \omega/\Delta E$, where ω is the laser frequency and ΔE is the energy spacing between the initial and neighboring states of the unperturbed system. Formally, the asymptotics can be derived by introducing ϵ into Eq. (1) explicitly via the substitution $F(t) \to F(\epsilon t)$. Here, we briefly summarize the results needed for the following.

The asymptotics of the solution to Eqs. (1) and (2) consists of two parts:

$$\psi(\mathbf{r},t) = \psi_a(\mathbf{r},t) + \psi_r(\mathbf{r},t). \tag{7}$$

The adiabatic part $\psi_a(\mathbf{r},t)$ describes the initial state distorted by the instantaneous laser field and adiabatically following its variation in time. In the presence of a static electric field equal to $\mathbf{F}(t)$ the initial bound state turns into a Siegert state (SS) satisfying

$$\left[-\tfrac{1}{2}\Delta + V(\mathbf{r}) + F(t)z - E_0(t)\right]\phi_0(\mathbf{r};t) = 0 \tag{8}$$

subject to regularity and outgoing-wave boundary conditions [28–30]. The SS we need is the solution to Eq. (8) which, being considered as a function of time, coincides with the initial bound state at zeros of $F(t)$, particularly at $t \to \pm\infty$. The SS eigenvalue $E_0(t)$ is complex,

$$E_0(t) = \mathcal{E}_0(t) - \frac{i}{2}\Gamma_0(t), \tag{9}$$

its real and imaginary parts defining the Stark-shifted energy and ionization rate of the state. The outgoing-wave part of the SS eigenfunction $\phi_0(\mathbf{r};t)$ describes electrons released from the system by either tunneling or over-the-barrier ionization in the field $\mathbf{F}(t)$. The flux of the outgoing electrons is directed opposite to the field, that is, toward $z \to \mp\infty$, where the signs $-$ and $+$ correspond to the cases $F(t) > 0$ and $F(t) < 0$, respectively. In this asymptotic region, $\phi_0(\mathbf{r};t)$ takes the form [28–30]

$$\phi_0(\mathbf{r};t)|_{z\to\mp\infty} = \int A_0(\mathbf{k}_\perp;t)e^{i\mathbf{k}_\perp\mathbf{r}_\perp}g(z,k_\perp;t)\frac{d\mathbf{k}_\perp}{(2\pi)^2}, \tag{10}$$

where $\mathbf{r}_\perp = (x,y)$, $\mathbf{k}_\perp = (k_x,k_y)$ is the transverse momentum of outgoing electrons, $A_0(\mathbf{k}_\perp;t)$ is the amplitude of the transverse momentum distribution (TMD) in the outgoing flux, and the function $g(z,k_\perp;t)$ represents an outgoing wave at $|z| \to \infty$:

$$g(z,k_\perp;t)|_{|z|\to\infty} = \frac{1}{|2F(t)z|^{1/4}}\exp\left(\frac{i|F(t)|^{1/2}|2z|^{3/2}}{3} + \frac{i\left[E_0(t) - \frac{1}{2}k_\perp^2\right]|2z|^{1/2}}{|F(t)|^{1/2}}\right). \tag{11}$$

Since the eigenvalue $E_0(t)$ has a negative imaginary part [see Eq. (9)], the eigenfunction $\phi_0(\mathbf{r};t)$ exponentially diverges in the asymptotic region. However, its normalization integral can be regularized by rotating the asymptotic part of the integration path in z into the complex z plane [28]. We assume that $\phi_0(\mathbf{r};t)$ is normalized to unity in this sense at all t. This defines the normalization of the TMD amplitude $A_0(\mathbf{k}_\perp;t)$. We will need this function taken at zero transverse momentum,

$$A_0(t) = A_0(\mathbf{k}_\perp = \mathbf{0};t). \tag{12}$$

Note that this quantity turns to zero if the polarization axis points along a nodal line of the unperturbed initial state $\phi_0(\mathbf{r})$. This is the case, e.g., for a linear molecule in a π state aligned along the polarization axis. Such specific symmetry cases require special treatment and are excluded from the present consideration. In other words, we assume that $A_0(t)$ does not vanish identically. Then, in the weak-field limit the amplitude (12) is related to the ionization rate [31]

$$|A_0(t)|^2 = \frac{4\pi\varkappa\Gamma_0(t)}{|F(t)|}, \quad |F(t)| \to 0, \tag{13}$$

where $\varkappa = \sqrt{2|E_0|}$. The adiabatic part in Eq. (7) is given in terms of the SS by [26]

$$\psi_a(\mathbf{r},t) = \phi_0(\mathbf{r};t)e^{-is_0(t)}, \tag{14}$$

where

$$s_0(t) = E_0 t + \int_{-\infty}^{t}[E_0(t') - E_0]\,dt'. \tag{15}$$

The exponent in Eq. (14) accounts for both the accumulation of an additional phase caused by the Stark shift of the initial state and its depletion due to ionization.

The adiabatic state (14) serves as a source of electrons. The rescattering part $\psi_r(\mathbf{r},t)$ in Eq. (7) describes electrons which, after a journey driven by the field, return to the parent ion for rescattering. Let us introduce a reference classical trajectory defined by

$$\dot{v}(t) = -F(t), \quad \dot{z}(t) = v(t), \tag{16a}$$

$$v(t \to -\infty) = z(t \to -\infty) = 0. \tag{16b}$$

In the limit $\epsilon \to 0$, the velocity $v(t)$ and coordinate $z(t)$ scale as $O(\epsilon^{-1})$ and $O(\epsilon^{-2})$, respectively, and the same holds for any trajectory satisfying Eqs. (16a) with different initial conditions. An electron released by the field begins its journey at a distance $O(\epsilon^0)$ from the origin. The range of the potential a is also $O(\epsilon^0)$. The spatial extent of the electron's trajectory, on the other hand, is $O(\epsilon^{-2})$. This means that the electron must return to the origin for rescattering to occur, that is, its trajectory must be closed. Closed trajectories in the present linear polarization case are collinear with the z axis. Consider a trajectory beginning at time t' and ending at time t. If this trajectory is closed, its initial and final velocities are determined by the moments t' and t and equal to

$$u_i(t,t') = v(t') - \frac{z(t) - z(t')}{t - t'}, \tag{17a}$$

$$u_f(t,t') = v(t) - \frac{z(t) - z(t')}{t - t'}, \tag{17b}$$

respectively. The classical action accumulated along the trajectory in this case is

$$\mathcal{S}(t,t') = \frac{[z(t) - z(t')]^2}{2(t - t')} - \frac{1}{2}\int_{t'}^{t} v^2(t'')dt''. \tag{18}$$

The initial velocity that an electron released from the system may have is $O(\epsilon^0)$, whereas in the general case

$u_i(t,t') = O(\epsilon^{-1})$. This means that the moment t' when ionization can occur for a given t must satisfy

$$u_i(t,t') = 0 \quad \rightarrow \quad t' = t_i(t). \tag{19}$$

We will need the derivatives of the function $t_i(t)$,

$$\frac{dt_i(t)}{dt} = \frac{-u_f(t)}{(t-t_i)F(t_i)}, \tag{20a}$$

$$\frac{d^2t_i(t)}{dt^2} = \frac{F(t)}{(t-t_i)F(t_i)} + \frac{2u_f(t)}{(t-t_i)^2F(t_i)} + \frac{[F(t_i)-(t-t_i)\dot{F}(t_i)]u_f^2(t)}{(t-t_i)^3F^3(t_i)}, \tag{20b}$$

where $t_i = t_i(t)$ and

$$u_f(t) \equiv u_f(t,t_i(t)) = v(t) - v(t_i(t)). \tag{21}$$

Closed trajectories with zero initial velocity [see Eq. (19)] are called *closed rescattering trajectories* (CRTs) [10]. Equation (21) gives the final velocity on a CRT, with which an electron arrives for rescattering. The above consideration shows that CRTs are the trajectories responsible for rescattering in the adiabatic regime. This classical picture indeed emerges in the derivation of the asymptotics of the rescattering part in Eq. (7) for $\epsilon \to 0$ from Eq. (1). The asymptotics is given by [26]

$$\psi_r(\mathbf{r},t) = \frac{-i}{2\pi}\sum_i \frac{A_0(t_i)}{|(t-t_i)^3F(t_i)|^{1/2}}\,\varphi(\mathbf{r};\mathbf{u}_f) \times \exp\,[i\mathcal{S}(t,t_i) - is_0(t_i)]. \tag{22}$$

Here, $t_i = t_i(t)$, $A_0(t_i)$ is the TMD amplitude from Eq. (12), $\varphi(\mathbf{r};\mathbf{u}_f)$ is the scattering state from Eqs. (6) taken at $\mathbf{k} = \mathbf{u}_f$, where $\mathbf{u}_f = u_f(t)\mathbf{e}_z$, and the summation runs over the different solutions to Eq. (19) for a given t. The second term in the exponent in Eq. (22) describes the quantum evolution of an electron in the adiabatic state (14) until the moment of ionization t_i, and the first term is the classical action (18) which the electron accumulates along a CRT after its release from the system.

The adiabatic theory [26] also yields the asymptotics of the ionization amplitude (5) for $\epsilon \to 0$. However, before turning to observables, we need to discuss the kinematics of rescattering.

C. Backward rescattering caustic

Consider an electron which is released from the system at time t_i, travels along a CRT, undergoes rescattering at time t_r, and then flies away with a final momentum $\mathbf{k}$. The momentum is represented by $\mathbf{k} = (\mathbf{k}_\perp, k_z)$, where $\mathbf{k}_\perp = k_\perp(\cos\varphi_k, \sin\varphi_k)$. To end up with a given momentum $\mathbf{k}$, the initial velocity of the electron after rescattering must be equal to $\mathbf{u}_i(t_r,\mathbf{k})$, where

$$\mathbf{u}_i(t,\mathbf{k}) = \mathbf{k} - [v_\infty - v(t)]\mathbf{e}_z \tag{23}$$

and $v_\infty = v(\infty)$. Thus, the moments t_i and t_r must satisfy

$$u_i(t_r,t_i) = 0, \tag{24a}$$

$$u_f^2(t_r,t_i) = \mathbf{u}_i^2(t_r,\mathbf{k}). \tag{24b}$$

The first of these equations amounts to the condition (19) for the CRT under consideration and the second one ensures conservation of energy in the rescattering event. The final velocity on the CRT, which is also the incident velocity of rescattering, is $\mathbf{u}_f = u_f\mathbf{e}_z$, where

$$u_f = v(t_r) - v(t_i). \tag{25}$$

Note that u_f has a sign which determines the direction of $\mathbf{u}_f$ with respect to the laboratory z axis. The scattering angles $\Omega = (\theta,\varphi)$ [see Eq. (6b)] are determined by

$$\cos\theta = \frac{k_z - v_\infty + v(t_r)}{u_f}, \quad \varphi = \varphi_k. \tag{26}$$

Equations (24)–(26) define the quantities t_i, t_r, u_f, and $\mathbf{u}_f$ characterizing the CRT and angles Ω characterizing the rescattering event as functions of $\mathbf{k}$; for brevity, we do not show this argument explicitly.

Equations (24) may have multiple solutions for t_i and t_r corresponding to the different CRTs leading to the same final momentum $\mathbf{k}$. As $\mathbf{k}$ varies, the CRTs may coalesce. The sets in the $\mathbf{k}$ space where this happens are called caustics. Consider one particular pair of long and short CRTs originating from the same half-cycle of the laser field [10]. They coalesce at a two-dimensional caustic which in the present case is a surface of revolution about the k_z axis. In the following, we consider a half-plane $\varphi_k = \text{const}$ with coordinates $(k_\perp,k_z)$. The section of the caustic by this half-plane is a curve $\mathbf{k}(\theta) = (k_\perp(\theta),k_z(\theta))$ which we parametrize by the scattering angle θ characterizing the coalesced CRTs. This curve will be somewhat loosely also called the caustic. At the caustic, the moments of ionization t_i and rescattering t_r defined by Eqs. (24) satisfy an additional equation which can be obtained by differentiating Eq. (24b) in t_r while treating t_i as a function of t_r defined by Eq. (24a):

$$2F(t_r)\sin^2(\theta/2) + \frac{u_f}{t_r - t_i} = 0. \tag{27}$$

To find the caustic, one needs to solve a system of equations (24a) and (27) with respect to t_i and t_r for a given θ using Eqs. (16), (17a), and (25). This defines functions $t_i(\theta)$, $t_r(\theta)$, and $u_f(\theta)$ giving the corresponding quantities at the caustic and the caustic itself,

$$k_\perp(\theta) = |u_f(\theta)|\sin\theta, \tag{28a}$$

$$k_z(\theta) = u_f(\theta)\cos\theta + v_\infty - v(t_r(\theta)). \tag{28b}$$

At the caustic, the final velocity on the CRT (the incident velocity of rescattering) is $\mathbf{u}_f(\theta) = u_f(\theta)\mathbf{e}_z$ and the initial velocity with which an electron flies away after rescattering is $\mathbf{u}_i(\theta) = \mathbf{u}_i(t_r(\theta),\mathbf{k}(\theta))$. These velocities have equal absolute values, $|\mathbf{u}_f(\theta)| = |\mathbf{u}_i(\theta)|$, and the angle between them is θ. Let us emphasize that the caustic $\mathbf{k}(\theta)$ is a classical object completely determined by the field $F(t)$ and independent of the target. We will consider only a part of the caustic adjacent to the backward rescattering direction $\theta = 180^\circ$; this part we call the BRC. The shape of a BRC for a typical few-cycle pulse to be considered in the calculations below is shown by the solid (black) line in Fig. 1.

Depending on the shape of the pulse $F(t)$, there may exist many different BRCs in the $(k_\perp,k_z)$ plane. We are interested in the vicinity of the outermost one, where the factorization of the PEMD occurs. For a monochromatic field of amplitude F and frequency ω, each half-cycle with positive

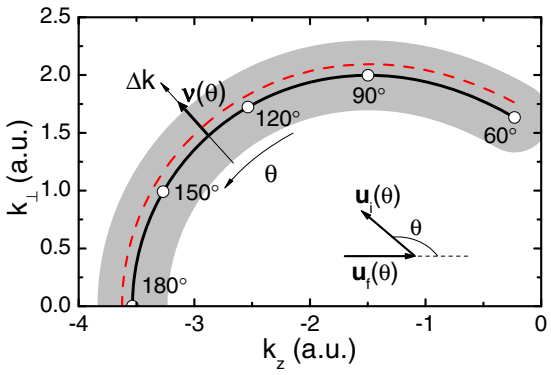

FIG. 1. Solid (black) line shows a classical BRC $\mathbf{k}(\theta)$ parametrized by the scattering angle θ [see Eqs. (28)]. The inset illustrates the incident velocity of rescattering $\mathbf{u}_f(\theta) = u_f(\theta)\mathbf{e}_z$ and the velocity after rescattering $\mathbf{u}_i(\theta)$ at the BRC. Curvilinear coordinates $(\theta, \Delta k)$ are introduced in the shaded strip near the BRC, with Δk measured along the external unit normal vector $\boldsymbol{\nu}(\theta)$ to the BRC. Dashed (red) line shows the projection of the corresponding quantum caustic $\tilde{\mathbf{k}}(\theta)$ [see Eqs. (42)] onto the real $(k_\perp, k_z)$ plane. The results are calculated for a pulse (46) with $F_0 = 0.1$ and $T = 200$ in the model considered in Sec. III A.

(negative) values of $F(t_i(\theta))$ produces the same BRC located at $k_z < 0$ ($k_z > 0$). In this case, the maximum of $|\mathbf{k}(\theta)|$ is attained at $\theta = 180^\circ$ and corresponds to the photoelectron energy $\mathbf{k}^2(180^\circ)/2 = 10.007 \times U_p$, where $U_p = F^2/4\omega^2$ is the ponderomotive potential [2]. For few-cycle pulses, the outermost BRC in the positive and negative k_z directions is produced by half-cycles containing the main maximum of the field of the corresponding sign. For definiteness, we consider this BRC in the interval $90^\circ \le \theta \le 180^\circ$, where PEMDs generated by typical pulses are determined by rescattered electrons; at smaller θ, it enters the region where direct electrons described by the adiabatic part in Eq. (7) dominate. Consider a narrow strip near the BRC shown by the shaded area in Fig. 1. Let $\boldsymbol{\nu}(\theta) = (\nu_\perp(\theta), \nu_z(\theta))$, $\boldsymbol{\nu}^2(\theta) = 1$ denote the external unit normal vector to the BRC, that is,

$$\boldsymbol{\nu}(\theta)\frac{d\mathbf{k}(\theta)}{d\theta} = 0, \quad \boldsymbol{\nu}(\theta)\frac{d^2\mathbf{k}(\theta)}{d\theta^2} \le 0. \tag{29}$$

It can be shown using Eq. (27) that

$$\boldsymbol{\nu}(\theta)\mathbf{u}_f(\theta) = |u_f(\theta)|\cos\theta. \tag{30}$$

This means that the angle between the normal $\boldsymbol{\nu}(\theta)$ and the positive direction of the k_z axis coincides with θ, if $u_f(\theta) > 0$, and with $\pi - \theta$, if $u_f(\theta) < 0$; in both cases $\nu_\perp = \sin\theta$. Any $\mathbf{k}$ located in the strip can be represented as

$$\mathbf{k} = \mathbf{k}(\theta) + \Delta k\,\boldsymbol{\nu}(\theta), \tag{31}$$

which amounts to

$$k_\perp = k_\perp(\theta) + \Delta k \nu_\perp(\theta), \tag{32a}$$

$$k_z = k_z(\theta) + \Delta k \nu_z(\theta). \tag{32b}$$

These equations define a transformation from Cartesian $(k_\perp, k_z)$ to curvilinear $(\theta, \Delta k)$ coordinates in the strip. The scattering angle θ is a coordinate along the BRC and the Δk is a coordinate across the BRC, the BRC coinciding with the coordinate line $\Delta k = 0$. Near $\theta = 180^\circ$, the BRC $\mathbf{k}(\theta)$ can be approximated by a circle of radius $|u_f(180^\circ)|$ with the center at $\mathbf{k} = [v_\infty - v(t_r(180^\circ))]\mathbf{e}_z$. Note that for a monochromatic field $|u_f(180^\circ)| = 1.247 \times F/\omega$ and $|v_\infty - v(t_r(180^\circ))| = 0.989 \times F/\omega$. This approximation implies that $t_i(\theta)$, $t_r(\theta)$, and $u_f(\theta)$ do not depend on θ and are substituted by their values at $\theta = 180^\circ$. We will call it the circular approximation below. This approximation was discussed in the Introduction; it was introduced in Ref. [3] and used in the extraction procedure in Refs. [11–18]. We mention that a similar kinematical approximation was used earlier for analyzing the momentum space wave function in a rescattering process [32]. However, the actual shape of the BRC differs from the circle and the quantities $t_i(\theta)$, $t_r(\theta)$, and $u_f(\theta)$ do depend on θ.

D. Factorization formula

In Ref. [26], we obtained another representation for the exact ionization amplitude (5) in terms of the exact solution to Eqs. (1) and (2),

$$I(\mathbf{k}) = \int_{-\infty}^{\infty} dt \int_\Sigma \mathbf{j}(\mathbf{r},t)\,d\boldsymbol{\Sigma}, \tag{33}$$

where

$$\mathbf{j}(\mathbf{r},t) = \frac{-i}{2}[e^{-i\mathcal{S}(\mathbf{r},t;\mathbf{k})}\nabla\psi(\mathbf{r},t) - \psi(\mathbf{r},t)\nabla e^{-i\mathcal{S}(\mathbf{r},t;\mathbf{k})}] \tag{34}$$

and

$$\mathcal{S}(\mathbf{r},t;\mathbf{k}) = \mathbf{u}_i(t,\mathbf{k})\mathbf{r} - \frac{1}{2}\int_0^t \mathbf{u}_i^2(t',\mathbf{k})\,dt'. \tag{35}$$

Here, $\mathbf{u}_i(t,\mathbf{k})$ is defined by Eq. (23), the spatial integration in Eq. (33) goes over any surface $\mathbf{r} \in \Sigma$ enclosing the region where the potential differs from zero, $d\boldsymbol{\Sigma}$ is the surface area element multiplied by the external unit normal vector to Σ, and we have omitted an unessential phase factor which does not modify the PEMD (4). Equation (33) is more convenient for calculating the ionization amplitude within the adiabatic theory. Substituting Eq. (7) into Eq. (34), one obtains $I(\mathbf{k}) = I_a(\mathbf{k}) + I_r(\mathbf{k})$, where the two terms correspond to the two terms in Eq. (7), respectively. The adiabatic part $I_a(\mathbf{k})$ describes direct electrons which do not interact with the parent ion after ionization, and the rescattering part $I_r(\mathbf{k})$ describes electrons which experience rescattering before arriving at a detector. The asymptotics of these two terms for $\epsilon \to 0$ were obtained in Ref. [26]. However, the formula for $I_r(\mathbf{k})$ presented therein was derived by treating the contributions from the different CRTs leading to the same final $\mathbf{k}$ separately, and hence it does not hold near a caustic. Here, we derive the uniform asymptotics of $I_r(\mathbf{k})$ which holds near a caustic.

We consider a pair of coalescing CRTs discussed in Sec. II C. Their joint contribution to $I_r(\mathbf{k})$ is denoted by $I_c(\mathbf{k})$. Substituting Eq. (22) into Eq. (34) and integrating over Σ in Eq. (33) using Eq. (6b), we obtain

$$I_c(\mathbf{k}) = \int_{-\infty}^{\infty} \frac{A_0(t_i)f(\mathbf{u}_f,\Omega)}{|(t-t_i)^3F(t_i)|^{1/2}}\,e^{iS_r(t,\mathbf{k})}\,dt, \tag{36}$$

where

$$S_r(t,\mathbf{k}) = \frac{1}{2}\int_0^t \mathbf{u}_i^2(t',\mathbf{k})\,dt' + \mathcal{S}(t,t_i) - s_0(t_i). \tag{37}$$

Here, $t_i = t_i(t)$, $\mathbf{u}_f = u_f(t)\mathbf{e}_z$, and the angles Ω define the direction of $\mathbf{u}_i(t,\mathbf{k})$ with respect to $\mathbf{u}_f$, namely, $\theta = \arccos\{[k_z - v_\infty + v(t)]/u_f(t)\}$ and $\varphi = \varphi_k$. The action (37) has two saddle points located near the moments of rescattering for the two coalescing CRTs. If $\mathbf{k}$ is far away from the caustic $\mathbf{k}(\theta)$, in calculating the integral in Eq. (36) using the steepest descent method the contributions from these saddle points can be treated separately. The result in this case reduces to the asymptotics obtained in Ref. [26]. If $\mathbf{k}$ is near the caustic, the saddle points are located close to each other near the moment of rescattering $t_r(\theta)$ at the caustic, and their contribution to the integral must be treated as a whole. We wish to calculate the uniform asymptotics of the integral (36) which holds in a strip near the caustic $\mathbf{k}(\theta)$ whose width in the direction of $\boldsymbol{\nu}(\theta)$ is specified below. The position of $\mathbf{k}$ in the strip is determined by coordinates $(\theta,\Delta k)$ (see Fig. 1). Let the caustic be characterized by the kinematic quantities $t_i(\theta)$, $t_r(\theta)$, $u_f(\theta)$, $\mathbf{u}_f(\theta)$, and $\mathbf{u}_i(\theta)$ defined in Sec. II C; for brevity, in the rest of this section we omit their argument. The action (37) as a function of t can be expanded near $t = t_r$. Using Eqs. (20), we obtain

$$\begin{aligned} S_r(t,\mathbf{k}) = {} & S_r(t_r,\mathbf{k}) + S_r'(\theta,\Delta k)\delta \\ & + \tfrac{1}{2}S_r''(\theta,\Delta k)\delta^2 + \tfrac{1}{6}S_r'''(\theta)\delta^3, \end{aligned} \tag{38}$$

where $\delta = t - t_r$ and

$$S_r'(\theta,\Delta k) = |u_f|\Delta k + \frac{E_0(t_i)u_f}{(t_r - t_i)F(t_i)}, \tag{39a}$$

$$S_r''(\theta,\Delta k) = -v_z(\theta)F(t_r)\Delta k, \tag{39b}$$

$$\begin{aligned} S_r'''(\theta) = u_f\Bigg[& 2\dot{F}(t_r)\sin^2(\theta/2) - \frac{3F(t_r)}{t_r - t_i} \\ & - \frac{3u_f}{(t_r - t_i)^2} - \frac{u_f^2}{(t_r - t_i)^3 F(t_i)}\Bigg]. \end{aligned} \tag{39c}$$

Here, we have consistently neglected terms of the order $O(\epsilon^1)$ and higher. Note that at the caustic $\Delta k = 0$, so the first term in the first derivative (39a) and the second derivative (39b) vanish. These vanishing terms originate from the first two classical terms in Eq. (37). The second term in Eq. (39a), which originates from the last quantum term in Eq. (37), does not vanish, and this has consequences. We mention that a different form of $S_r'''(\theta)$ given by Eq. (6) in Ref. [25] can be reduced to Eq. (39c) using Eqs. (20). Substituting the expansion (38) into Eq. (36) and calculating the integral, we obtain

$$\begin{aligned} I_c(\mathbf{k}) = {} & \mathrm{Ai}(\alpha(\theta)[\mathbf{k} - \tilde{\mathbf{k}}(\theta)]\boldsymbol{\nu}(\theta)) \\ & \times \left(\frac{2}{S_r'''(\theta)}\right)^{1/3} \frac{2\pi A_0(t_i) f(\mathbf{u}_f,\Omega)}{|(t_r - t_i)^3 F(t_i)|^{1/2}}\, e^{iS_r(\tilde{t}_r,\mathbf{k})}. \end{aligned} \tag{40}$$

Here, $\mathrm{Ai}(z)$ is the Airy function [33], its argument is defined by

$$\alpha(\theta) = \left(\frac{2}{S_r'''(\theta)}\right)^{1/3} |u_f| \tag{41}$$

and

$$\tilde{\mathbf{k}}(\theta) = \mathbf{k}(\theta) + q(\theta)\boldsymbol{\nu}(\theta), \tag{42a}$$

$$q(\theta) = \frac{-E_0(t_i)}{(t_r - t_i)|F(t_i)|}, \tag{42b}$$

the scattering angles are $\Omega = (\theta,\varphi_k)$, and $\tilde{t}_r = \tilde{t}_r(\theta,\Delta k)$, where

$$\tilde{t}_r(\theta,\Delta k) = t_r - \frac{S_r''(\theta,\Delta k)}{S_r'''(\theta)} \tag{43}$$

is the point where the second derivative of Eq. (38) in t vanishes. The two saddle points of the action (38) coalesce along the curve $\mathbf{k} = \tilde{\mathbf{k}}(\theta)$, where the argument of the Airy function in Eq. (40) turns to zero. We call $\tilde{\mathbf{k}}(\theta)$ the quantum caustic because the shift of this curve with respect to the classical caustic $\mathbf{k}(\theta)$ given by Eqs. (42) is caused by the last quantum term in Eq. (37). Note that the shift (42b) depends on the SS eigenvalue $E_0(t_i)$, so the quantum caustic is target dependent. Also note that it is complex because the eigenvalue (9) is complex, so the quantum caustic $\tilde{\mathbf{k}}(\theta)$ does not belong to the real $(k_\perp,k_z)$ plane; its projection onto this plane is illustrated in Fig. 1. The real part of $q(\theta)$ is positive, so $\tilde{\mathbf{k}}(\theta)$ lies outside $\mathbf{k}(\theta)$. We have $q(\theta) = O(\epsilon^1)$, so the shift disappears in the limit $\epsilon \to 0$, and in this sense it represents a nonadiabatic effect. However, the period of oscillations of the Airy factor in Eq. (40) as a function of Δk near the BRC is also $O(\epsilon^1)$ because $\alpha(\theta) = O(\epsilon^{-1})$, so the shift can never be neglected. Equations (42) generalize our previous result obtained for a one-dimensional model [10] to the three-dimensional case, that is, to arbitrary scattering angles θ. In the weak-field limit $E_0(t_i) \approx E_0$; in this approximation, the shift (42b) for a monochromatic pulse at $\theta = 180^\circ$ agrees with a shift in the energy domain obtained in Ref. [34]. Equation (40) is the main analytical result of this work. This asymptotics holds provided that the distance between the two saddle points of the action (38) is $o(\epsilon^{-1})$, which is the case in a strip of width $\Delta k = o(\epsilon^{-1})$ including both classical $\mathbf{k}(\theta)$ and quantum $\tilde{\mathbf{k}}(\theta)$ caustics.

The following comment regarding the technique of the derivation may be in order here. The appearance of the Airy function in the evaluation of an integral with two coalescing saddle points by the steepest descent method is well known in mathematics [35]. In physics, this technique is used, e.g., in the standard textbook treatment of caustics in optics [36]. In the context of strong-field physics, to the best of our knowledge, the technique was first applied in Ref. [37]. More recently, the appearance of the Airy function was mentioned in passing in the analysis of the cutoff region of the spectrum of high-order harmonics [38]; the issue was pedagogically discussed in the Appendix C of Ref. [39]. In the description of the contribution to the PEMD from backward rescattered electrons, the Airy function first appeared in Ref. [40]. Not surprisingly, it has also appeared in all subsequent analytical treatments of the subject [5,7–10]. However, we emphasize that its argument in all previous treatments differs from that in Eq. (40).

Equation (40) describes joined contribution of any pair of coalescing CRTs near the corresponding caustic. Consider the vicinity of the outermost BRC. As discussed above, in this region the contribution to the total ionization amplitude $I(\mathbf{k})$ from direct electrons represented by $I_a(\mathbf{k})$ can be neglected. The amplitude (40) quickly decays outside the corresponding

caustic because of the Airy function factor. Hence, near the outermost BRC one can also neglect all contributions to $I_r(\mathbf{k})$ except for the only one term $I_c(\mathbf{k})$ representing the coalescing CRTs. The PEMD $P(\mathbf{k})$ in this region can be approximated by $P_c(\mathbf{k}) = |I_c(\mathbf{k})|^2$. Using Eq. (40), we obtain

$$P_c(\mathbf{k}) = |f(\mathbf{u}_f,\Omega)|^2 W(\theta,\Delta k), \tag{44}$$

where

$$W(\theta,\Delta k) = |\mathrm{Ai}\,(\alpha(\theta)[\Delta k - q(\theta)])|^2 \left|\frac{2}{S_r'''(\theta)}\right|^{2/3} \times \frac{4\pi^2 |A_0(t_i)|^2}{(t_r - t_i)^3 |F(t_i)|} \exp\left[-\int_{-\infty}^{t_i} \Gamma_0(t)\,dt\right]. \tag{45}$$

This is the FF foreseen in Ref. [3]. The first factor in Eq. (44) is the DCS for rescattering at the BRC; let us recall that $\mathbf{u}_f = u_f(\theta)\mathbf{e}_z$ and $\Omega = (\theta,\varphi_k)$. The second factor is the RWP; we recall that in Eq. (45), as well as in Eqs. (39c), (41), and (42b) defining the notation therein, we have omitted the argument of $t_i(\theta)$, $t_r(\theta)$, and $u_f(\theta)$. The last exponential factor in Eq. (45) accounts for the depletion of the adiabatic state (14) before the moment of ionization t_i, the ionization step is represented by the TMD amplitude (12) squared, and the other factors describe propagation along the CRT. Equation (44) defines the PEMD as a function of coordinates $(\theta,\Delta k,\varphi_k)$ in the vicinity of the outermost BRC in the $\mathbf{k}$ space. Note that only the Airy function in the RWP (45) depends on the transverse with respect to the BRC coordinate Δk. This formula is derived in the adiabatic approximation, that is, it becomes exact as the adiabatic parameter ϵ tends to zero, assuming that the other parameters characterizing the target and pulse are kept fixed.

To close this section, let us indicate the differences between Eq. (44) and the previous version of the FF given in Ref. [25]: (a) Equation (44) describes the PEMD in a strip near the BRC, the dependence of the PEMD on the transverse coordinate Δk in the strip being described by the RWP (45), while in Ref. [25] the FF was given only at the BRC. (b) Equation (44) accounts for a quantum shift of the caustic, which is represented by the term $q(\theta)$ in the argument of the Airy function in Eq. (45). This shift was not discussed in Ref. [25]. (c) Equation (44) does not rely on the weak-field approximation (13) used in Ref. [25], and hence applies to really strong over-the-barrier fields. The importance of this strong-field effect is illustrated in Sec. III D. (d) Equation (44) holds for general finite-range potentials without any symmetry, while in Ref. [25] only spherically symmetric potentials were considered. This generalization enables one to extract the dependence of the DCS for molecular targets on both scattering angles θ and φ.

III. ILLUSTRATIVE CALCULATIONS AND DISCUSSION

In this section we illustrate the quantitative performance of the FF by calculations. The results obtained from Eq. (44) will be referred to as AA, which stands for the adiabatic approximation. We compare them with the TDSE results obtained by solving Eqs. (1) and (2). We consider two-cycle pulses of the form

$$F(t) = -F_0 \cos(4\pi t/T)\exp[-(2t/T)^2] \tag{46}$$

characterized by the amplitude F_0 and duration T. Typical values of these parameters $F_0 = 0.1$ and $T = 200$ considered below correspond to the intensity 3.5×10^{14} W/cm^2 and wavelength 725 nm, respectively. The adiabatic parameter ϵ for such pulses is inversely proportional to T. One of the goals is to confirm that the AA results converge to the TDSE results as T grows while F_0 is kept fixed, and this holds in both tunneling and over-the-barrier regimes of ionization. Another goal is to illustrate the convergence for the different potentials, including potentials with a Coulomb tail. In the calculations we consider only spherically symmetric potentials. The PEMD $P(\mathbf{k})$ in this case is axially symmetric about the k_z axis and will be denoted by $P(k_\perp,k_z)$. The SS information needed to implement Eq. (44) is calculated using the method developed in Ref. [28]. The TDSE results are obtained using a program described in Ref. [41].

The BRC discussed below results from the coalescence of CRTs originating from the central cycle of the field (46) containing $t = 0$. For this BRC, the moment of ionization $t_i(\theta)$ lies slightly to the right of $t = -T/4$ and the moment of rescattering $t_r(\theta)$ lies near $t = +T/8$. The actual values of $t_i(\theta)$ and $t_r(\theta)$ as functions of θ can be found by solving Eqs. (24a) and (27) using the Newton method. Then, the coordinates of the BRC $\mathbf{k}(\theta) = (k_\perp(\theta),k_z(\theta))$ can be obtained from Eqs. (28). Since in the present case $F(t_i(\theta)) > 0$, the curve $\mathbf{k}(\theta)$ lies in the region $k_z < 0$. This curve calculated for a pulse with $F_0 = 0.1$ and $T = 200$ is shown in Fig. 1. The FF (44) applies in the vicinity of the BRC: this is the region we focus on in the following discussion. This region is parametrized by coordinates $(\theta,\Delta k)$ defined by Eqs. (32). We will discuss cuts of the PEMD $P(k_\perp,k_z)$ across the BRC at several fixed values of θ as functions of Δk and cuts along the BRC, at $\Delta k = 0$, as functions of θ. The cuts obtained from the TDSE results are denoted by $P(\Delta k)$ and $P(\theta)$, respectively, and the corresponding cuts obtained from Eq. (44) are denoted by $P_c(\Delta k)$ and $P_c(\theta)$. For the given pulse shape (46), the functions $k_\perp(\theta)$ and $k_z(\theta)$ depend on the pulse parameters F_0 and T only via a common factor F_0T, that is, being divided by this factor they become independent of F_0 and T. Table I presents such scaled coordinates of the four points at the BRC corresponding to the four values of θ considered in the calculations. In the present case, the shape of the BRC is rather close to a circle at $\theta > 90^\circ$, the departure from the circular approximation becomes more prominent only at smaller θ. Since $u_f(\theta) > 0$ (see Fig. 1), the angle between the normal $\boldsymbol{\nu}(\theta)$ to the BRC and the positive direction of the k_z axis coincides with θ [see Eq. (30)]. The Δk coordinate is measured along the normal $\boldsymbol{\nu}(\theta)$, so the information presented in the table enables one to

TABLE I. Scaled coordinates of the four points at the BRC $\mathbf{k}(\theta)$ corresponding to the four values of θ considered in the present calculations.

θ	$(F_0T)^{-1}k_\perp(\theta)$	$(F_0T)^{-1}k_z(\theta)$
90°	0.09989	−0.0748
120°	0.08613	−0.1268
150°	0.04953	−0.1635
180°	0	−0.1767

reconstruct the $(k_\perp,k_z)$ coordinates of the cuts at fixed θ to be considered below.

A. Validation of the factorization formula for a finite-range potential

We begin with the validation of the FF for a finite-range potential, that is, in the situation for which it was derived. We consider a screened Coulomb potential

$$V(r) = -\frac{\exp[-(r/a)^2]}{r}. \tag{47}$$

In this section the screening parameter is set to $a = 10$. As the initial state we use the $1s$ state; its energy is $E_0 \approx -0.485\,483$. The same potential and initial state were used in the illustrative calculations in Ref. [26]. The critical field indicating a boundary between the tunneling and over-the-barrier regimes of ionization in the present case is $F_c \approx 0.12$.

We first consider three pulses with the same amplitude $F_0 = 0.1 < F_c$ belonging to the tunneling regime and growing duration T. The results for these pulses are shown in the three columns in Fig. 2. The PEMDs obtained by solving the TDSE are shown in the top row of the figure. They have a sharp boundary in the region $k_z < 0$ which is determined by the BRC under consideration. This BRC for the pulse with $T = 200$ (the right column in Fig. 2) is shown in Fig. 1. The other rows in Fig. 2 show cuts of the PEMDs across the BRC at four values of the scattering angle θ as functions of Δk. The solid (black) lines show the TDSE results and the dashed (red) lines show the AA results. To bring the results in the different panels to a common scale, the TDSE and AA results in each panel are divided by the same factor $P_0 = P_c(\Delta k = 0)$ giving the corresponding value of the AA cut at $\Delta k = 0$, so that the AA curve always passes through unity at $\Delta k = 0$. The main conclusion to be drawn from the figure is that the AA results do converge to the TDSE results as T grows. Note,

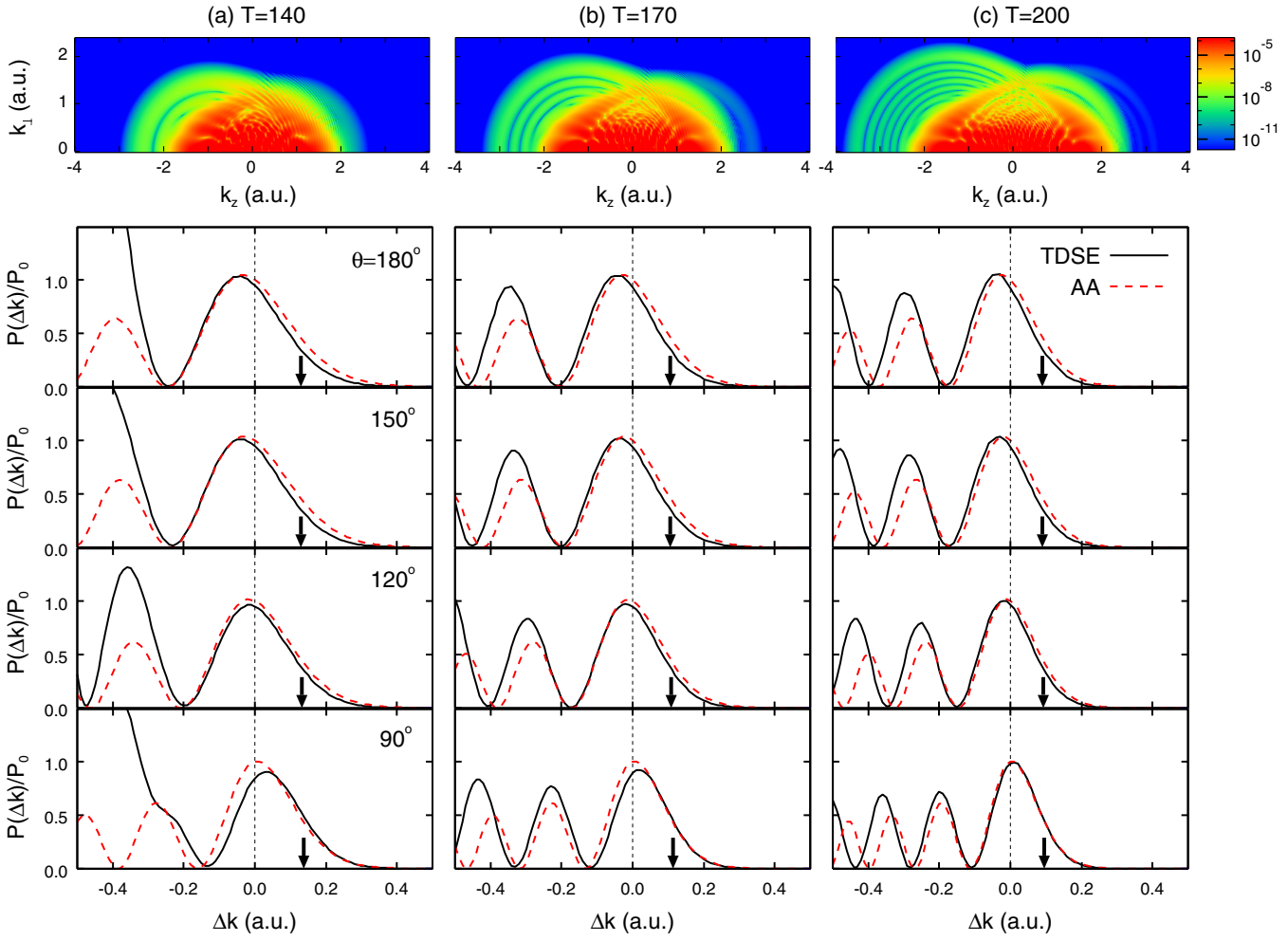

FIG. 2. PEMDs for ionization from the $1s$ state in a finite-range potential (47) with $a = 10$ generated by pulses (46) with the same amplitude $F_0 = 0.1$ belonging to the tunneling regime and three durations T indicated in the titles of the columns. The top row shows TDSE results for $P(k_\perp,k_z)$ obtained by solving Eqs. (1) and (2). The BRC we are interested in goes along the boundary of the PEMDs in the region $k_z < 0$ (compare with Fig. 1). Solid (black) lines in the other rows show cuts $P(\Delta k)$ of the TDSE PEMDs across the BRC at four values of θ indicated in the left column as functions of Δk. Dashed (red) lines show the cuts $P_c(\Delta k)$ obtained in the adiabatic approximation from the FF (44). The TDSE and AA results in each panel are divided by the same factor $P_0 = P_c(\Delta k = 0)$ giving the corresponding value of the AA cut. The vertical dotted lines at $\Delta k = 0$ show the position of the BRC. The arrows located at $\Delta k = \mathrm{Re}[q(\theta)]$ indicate the position of the real part of the quantum caustic defined by Eqs. (42). The total ionization probability P_{ion} for these pulses is (a) 0.20, (b) 0.22, and (c) 0.23.

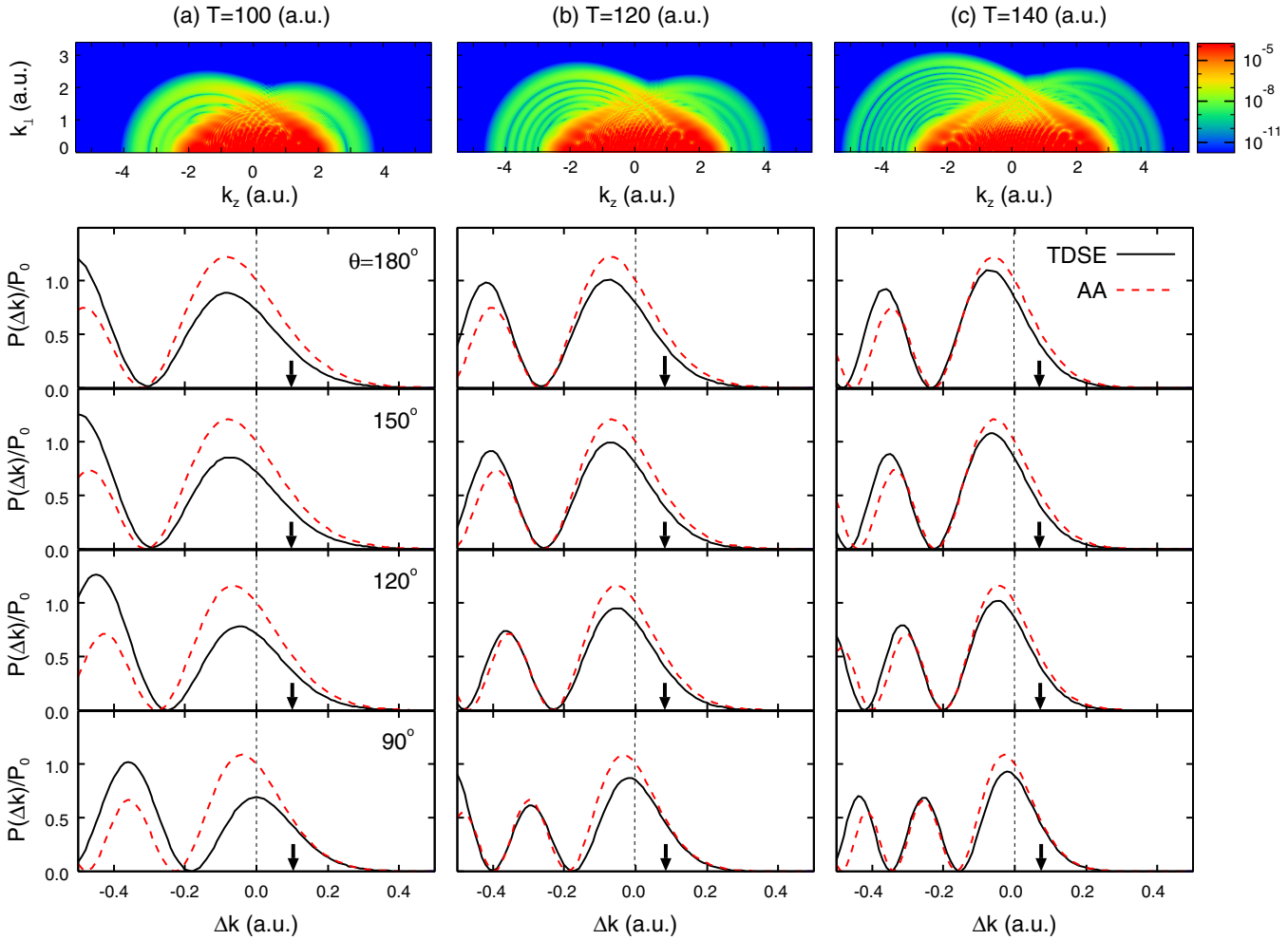

FIG. 3. Same as in Fig. 2, but for pulses with an over-the-barrier amplitude $F_0 = 0.2$. The total ionization probability $P_{\rm ion}$ for these pulses is (a) 0.90, (b) 0.95, and (c) 0.96.

importantly, that the cuts of the PEMDs in Fig. 2 are shown on a linear scale, so the level of agreement between numerical and analytical results is really impressive. As expected, the agreement becomes better near the BRC located at $\Delta k = 0$. For example, for $T = 200$, the difference between the TDSE and AA results at $\Delta k = 0$ varies from 8% at $\theta = 180^\circ$ to 2% at $\theta = 90^\circ$. The arrows indicate the position of the real part of the quantum caustic defined by Eqs. (42); this caustic for the pulse with $T = 200$ is shown in Fig. 1. The quantum shift $q(\theta)$ in the argument of the Airy function in Eq. (45) decreases as T grows, but remains of the same order $O(\epsilon^1)$ as the width of the rightmost maximum in the oscillatory dependence of the cuts $P(\Delta k)$ on Δk. It is clear that accounting for this shift is essential for achieving the agreement seen in Fig. 2.

Figure 3 presents similar results, but for pulses with an amplitude $F_0 = 0.2 > F_c$ belonging to the over-the-barrier regime. Because of technical difficulties in the calculations, in this case we consider somewhat smaller values of T. For $T = 140$, the difference between the TDSE and AA results at $\Delta k = 0$ varies from 20% at $\theta = 180^\circ$ to 12% at $\theta = 90^\circ$. Although this difference is larger than in the previous case, because of the smaller values of T considered, the results are again seen to converge as T grows, and this is the main feature we wish to demonstrate. Note that the total ionization probability for the present pulses exceeds 90%, and even for such a violent field-atom interaction Eq. (44) works well. We recall that the adiabatic theory [26] in general, and Eq. (44) in particular, apply to arbitrary field amplitudes, provided that the adiabatic parameter ϵ is sufficiently small, and this is confirmed by the results shown in Figs. 2 and 3. These results validate the FF (44) for finite-range potentials.

B. Toward potentials with a Coulomb tail

Realistic potentials modeling the interaction of an active electron with the parent ion in neutral atoms and molecules have a Coulomb tail. So, for applications it is important to demonstrate that Eq. (44) applies in this case too. We first give analytical arguments supporting the possibility to extend Eq. (44) to Coulomb-tail potentials and then confirm this by calculations.

The asymptotics of the adiabatic part in Eq. (7) given by Eq. (14) holds for finite-range as well as Coulomb-tail potentials [26]. But, the asymptotics of the rescattering part in Eq. (7) given by Eq. (22) and formula (33) for the exact ionization amplitude were derived in Ref. [26] relying on

the assumption that the potential has a finite range. The problem with Eq. (22) in the case of Coulomb-tail potentials stems from the divergence of the scattering amplitude in the forward direction; this prevents the step from Eq. (99) to (103) in Ref. [26]. However, this problem does not arise if one considers only near-backward rescattered electrons. The problem with Eq. (33) is that this formula does not account for the logarithmic Coulomb phase of the final state in the Coulomb-tail case. However, this phase is the same for both contributions to $I_c(\mathbf{k})$ from coalescing CRTs near the BRC, so it disappears in Eq. (44). These arguments suggest that Eq. (44) should hold also for Coulomb-tail potentials.

We demonstrate that this is indeed the case by considering potentials (47) with growing value of the screening parameter a. We begin with $a = 10$ treated in the previous subsection and proceed to $a = \infty$, which corresponds to the pure Coulomb potential. As the initial state we again use the $1s$ state. To confirm that the Coulomb tail does not affect the shape of the PEMD in the vicinity of the BRC, where Eq. (44) applies, we need to show that the accurate PEMD obtained by solving the TDSE converges in this region as a grows. We first consider a pulse in the tunneling regime with $F_0 = 0.1$ and $T = 200$, as in the right column in Fig. 2. The upper panel in Fig. 4 shows TDSE results for the cuts of PEMDs calculated for several values of a as functions of Δk at a representative value of the scattering angle $\theta = 150^\circ$, as in the third row in Fig. 2. The results clearly converge. For the present pulse, the convergence is achieved at $a = 50$, which means that the tail of the Coulomb potential extending beyond $r \sim 50$ does not affect the shape of the PEMD in the region under consideration. The AA results obtained from Eq. (44) are shown in the lower panel of the figure. They demonstrate a very similar convergence behavior.

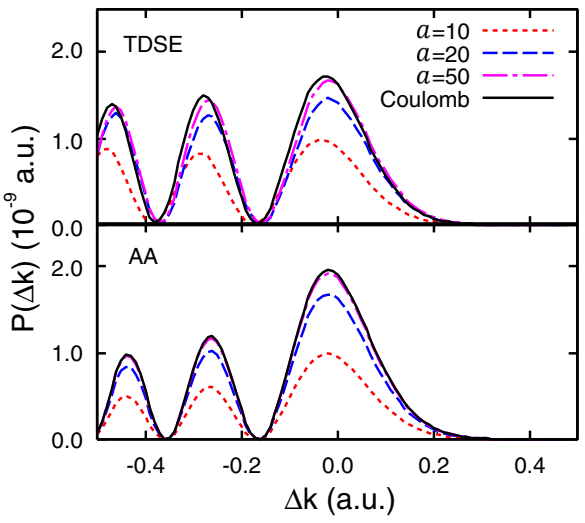

FIG. 4. Cuts of the PEMDs for ionization from the $1s$ state in potentials (47) with different values of the screening parameter a. The Coulomb potential corresponds to $a = \infty$. The PEMDs are generated by pulses (46) with the amplitude $F_0 = 0.1$ and duration $T = 200$, as in the right column in Fig. 2. The cuts are shown as functions of Δk at $\theta = 150^\circ$, as in the third row in Fig. 2. The upper and lower panels show the TDSE and AA results, respectively. Note that here absolute (not divided by any factor) results are shown.

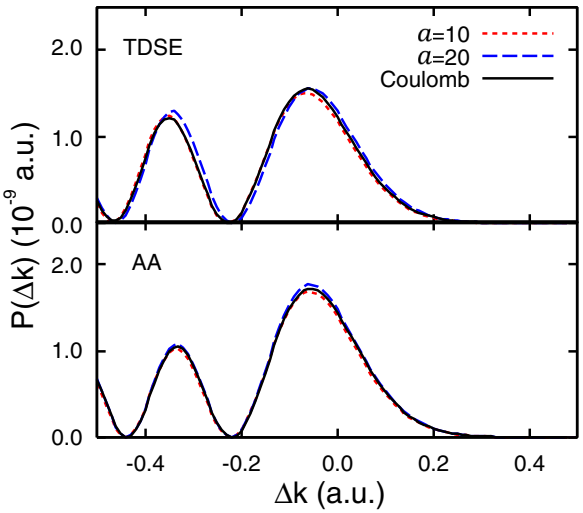

FIG. 5. Same as in Fig. 4, but for pulses with $F_0 = 0.2$ and $T = 140$, as in the right column in Fig. 3. The cuts are shown as functions of Δk at $\theta = 150^\circ$, as in the third row in Fig. 3.

The Coulomb results in this case are obtained by using the Coulomb DCS. The AA and TDSE results for the same a are close to each other, the difference between them is similar to that seen in the right column in Fig. 2, and it was shown to decrease as the pulse duration T grows.

Figure 5 shows similar results for a pulse in the over-the-barrier regime with $F_0 = 0.2$ and $T = 140$, as in the right column in Fig. 3. In this case, the finite-range and Coulomb results converge already for $a = 10$. The slower convergence for weaker fields is explained as follows. The main dependence on the screening parameter a in Eq. (44) comes from the factor $|A_0(t_i)|^2$ in Eq. (45), which describes the ionization step. In the weak-field limit this factor is related to the ionization rate [see Eq. (13)]. The weak-field asymptotics of the rates of ionization from finite-range and Coulomb-tail potentials have different powers of the field in the preexponential factor [31], which strongly affects their values. For stronger fields, the ionization rate as well as the factor $|A_0(t_i)|^2$ are less affected by the long-range behavior of the potential.

Summarizing, the results in Figs. 4 and 5 confirm that PEMDs near the outermost BRC are not sensitive to the Coulomb tail of the potential and, therefore, Eq. (44) applies also to potentials with a Coulomb tail. Note that in other parts of the momentum space, PEMDs may be affected by the Coulomb tail.

C. Realistic atomic potentials

We now consider realistic atomic potentials with a Coulomb tail. We begin with the discussion of ionization from the $5p$ state of Xe described by the potential defined in Ref. [42]. The results obtained for three pulses with the same amplitude $F_0 = 0.06$ belonging to the tunneling regime and growing duration are shown in Fig. 6. The top row in the figure shows PEMDs obtained by solving the TDSE. The middle row shows cuts of the PEMDs across the BRC at $\theta = 180^\circ$. These results are similar to the cuts shown in Figs. 2 and 3. The TDSE and AA results in each panel are divided by

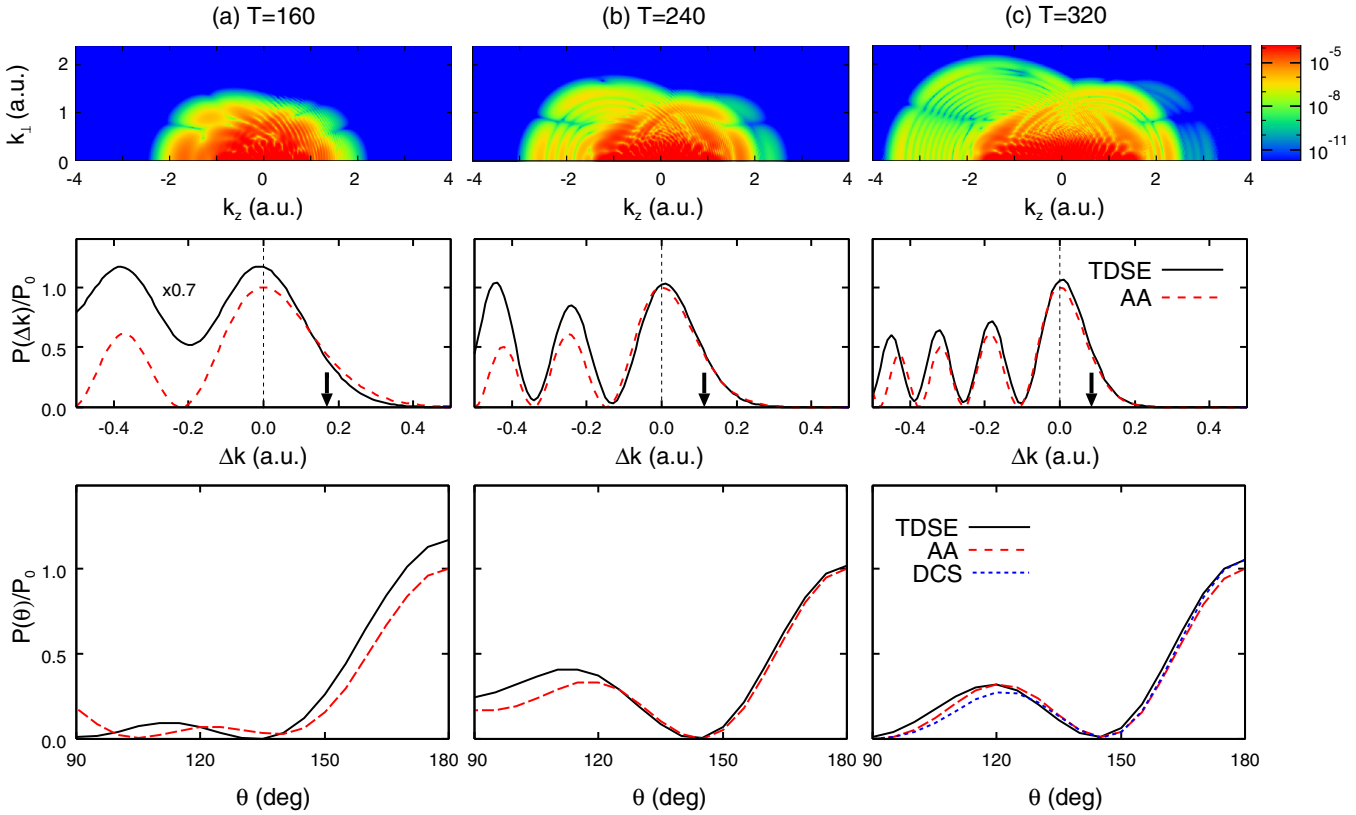

FIG. 6. PEMDs for ionization from the $5p$ state of Xe described by the potential from Ref. [42] generated by pulses (46) with the same amplitude $F_0 = 0.06$ belonging to the tunneling regime and three durations T indicated in the titles of the columns. The top row shows TDSE results for $P(k_\perp,k_z)$. In the middle row: solid (black) lines show cuts $P(\Delta k)$ of the TDSE PEMDs across the BRC at $\theta = 180^\circ$ as functions of Δk and dashed (red) lines show the cuts $P_c(\Delta k)$ obtained from Eq. (44). The TDSE and AA results in each panel are divided by the same factor $P_0 = P_c(\Delta k = 0)$ giving the corresponding value of the AA cut, as in Figs. 2 and 3. Note that in the left panel the TDSE results are additionally multiplied by 0.7. The vertical dotted lines show the position of the BRC and the arrows indicate the position of the real part of the quantum caustic. In the bottom row: solid (black) lines show cuts $P(\theta)$ of the TDSE PEMDs along the BRC, at $\Delta k = 0$, as functions of θ and dashed (red) lines show the cuts $P_c(\theta)$ obtained from Eq. (44). The TDSE and AA results in each panel are divided by the same factor $P_0 = P_c(\theta = 180^\circ)$ giving the corresponding value of the AA cut. The dotted (blue) line in the right panel shows the DCS as a function of θ at a constant incident momentum $|u_f(180^\circ)|$. The DCS is multiplied by a factor which brings its value at $\theta = 180^\circ$ in coincidence with the TDSE curve. The total ionization probability $P_{\rm ion}$ for these pulses is (a) 0.12, (b) 0.15, and (c) 0.18.

the same factor $P_0 = P_c(\Delta k = 0)$ giving the corresponding value of the AA cut at $\Delta k = 0$, so that the AA curve always passes through unity at $\Delta k = 0$. The bottom row shows cuts of the PEMDs along the BRC, that is, at $\Delta k = 0$. In this case, the TDSE and AA results in each panel are divided by the same factor $P_0 = P_c(\theta = 180^\circ)$ giving the corresponding value of the AA cut at $\theta = 180^\circ$, so that the AA curve always passes through unity at $\theta = 180^\circ$. Figure 7 shows similar results for pulses with an amplitude $F_0 = 0.2$ belonging to the over-the-barrier regime. In both figures, the AA and TDSE results are again seen to converge as T grows, and this is the main feature we wish to emphasize. For the weaker pulses in Fig. 6, the onset of the adiabatic regime is passed near $T = 240$, which corresponds to the wavelength of 870 nm. For the stronger pulses in Fig. 7, the adiabatic regime is reached at smaller T. Note that good agreement between the AA and TDSE results is achieved even though the total ionization probability for the latter pulses exceeds 90%. Figures 6 and 7 confirm that Eq. (44) applies to realistic atomic potentials.

Having confirmed that Eq. (44) works quantitatively, we now discuss its main virtue for applications in strong-field physics. The FF (44) predicts that by dividing a PEMD taken along the outermost BRC by the RWP (45) one obtains the corresponding DCS. This is the extraction procedure resulting from the present theory. Since the RWP at the BRC is a given function of θ, the agreement between the DCSs extracted in this way from the present PEMDs for Xe obtained by solving the TDSE and the results of independent scattering calculations is the same as the agreement between the TDSE and AA results shown in the bottom rows in Figs. 6 and 7. This agreement is good and becomes better as T grows. In Fig. 8 we show similar cuts of PEMDs along the BRC calculated for different targets. We consider ionization from the $1s$ state in H and the outer shell of noble gas atoms, namely, $2p$ state in Ne, $3p$ state in Ar, and $4p$ state in Kr, described by potentials defined in Ref. [42]. The agreement for H is virtually perfect, while for the other atoms some difference can still be seen for the present pulses. These results illustrate the quantitative performance of the extraction procedure based on Eqs. (44) and (45).

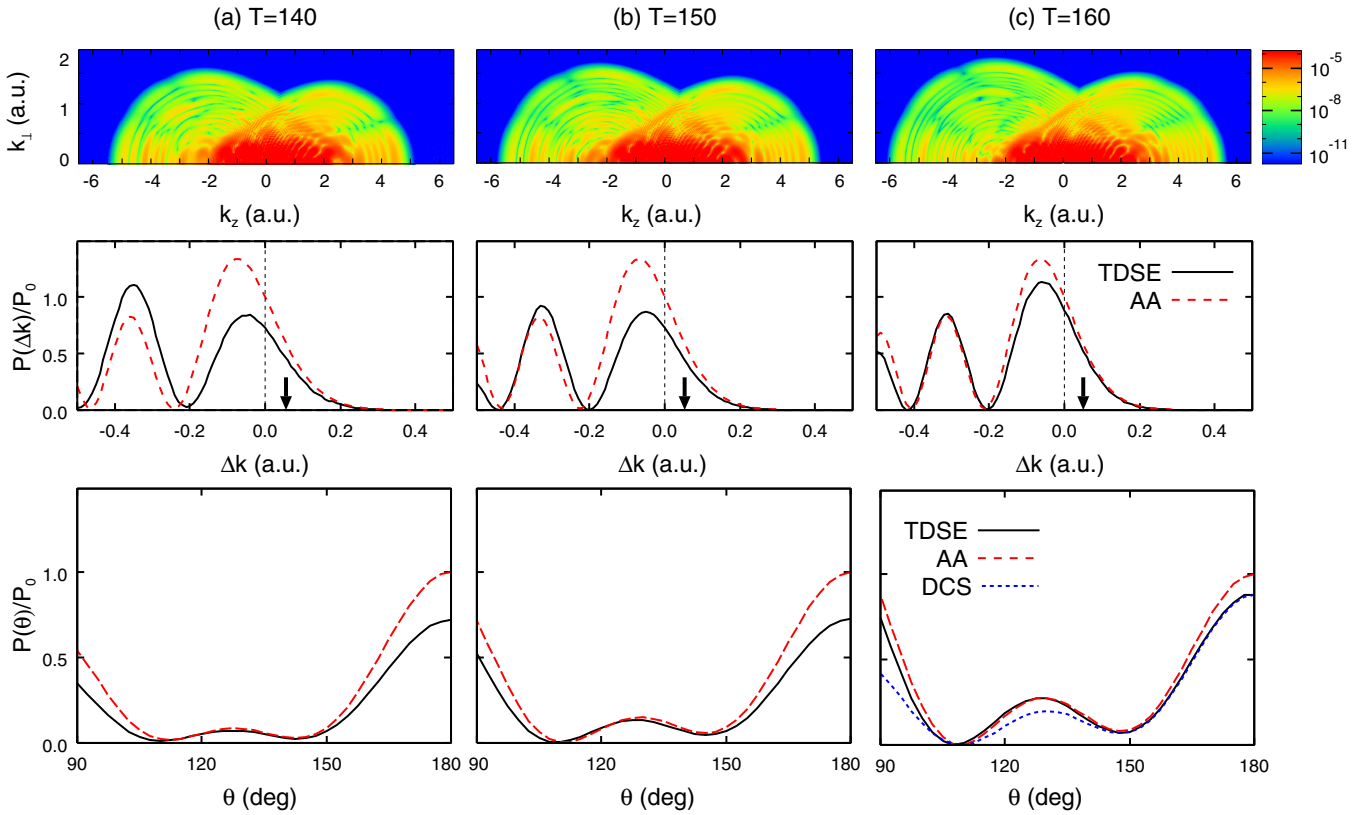

FIG. 7. Same as in Fig. 6, but for pulses with an over-the-barrier amplitude $F_0 = 0.2$. The total ionization probability $P_{\rm ion}$ for these pulses is (a) 0.94, (b) 0.94, and (c) 0.95.

The AA results shown in the bottom rows in Figs. 6 and 7 and in Fig. 8 are obtained from Eq. (44) by taking into account the correct dependence of the DCS and RWP on both the incident momentum of rescattering $|u_f(\theta)|$ and the scattering angle θ along the BRC. In the circular approximation discussed in the Introduction and in the end of Sec. II C, which was used in the extraction procedure in Refs. [3,11–18], the incident momentum is taken to be equal to $|u_f(\theta = 180^\circ)|$ and the RWP is assumed to be a constant. It is instructive to compare this approximation with the present AA results. The dotted (blue) lines in the bottom right panels in Figs. 6 and 7 and in Fig. 8 show the DCS at constant incident momentum $|u_f(180^\circ)|$ as a function of the scattering angle θ. To make the comparison with the TDSE and AA PEMDs possible, the DCS in each case is multiplied by a factor which brings its value at $\theta = 180^\circ$ in coincidence with the TDSE curve: this is what one would obtain in the circular approximation. Although in all the cases the DCS curves look almost as good as the AA results, which is partially explained by the fact that the BRC for the present pulses is very close to a circle, we would like to emphasize the following. First, the circular approximation enables one to extract a DCS only up to an unknown incident-momentum-dependent factor, while Eq. (44) yields the correct absolute values of the DCS. Second, Eq. (44) is shown to work quantitatively from the onset of the adiabatic regime corresponding to the wavelength about 800 nm and to become more accurate as the wavelength grows, while the errors incurred by the circular approximation do not decrease at longer wavelengths. Third, although the improvement of Eq. (44) over the circular approximation demonstrated in Figs. 6–8 is not large quantitatively, there is a definite improvement in each case, and this becomes essential for current applications as experimental techniques progress toward detecting fine multielectron effects in DCSs.

D. Strong-field effects

The RWP (45) depends on the target through three quantities: the energy $E_0(t_i)$ of the adiabatic state (14) at the moment of ionization $t_i = t_i(\theta)$ at the BRC defining the quantum shift (42b) of the caustic, the factor $|A_0(t_i)|^2$ describing the ionization step, and the ionization rate $\Gamma_0(t)$ defining the exponential depletion factor. All these quantities are properties of the adiabatic SS defined by Eq. (8), and therefore they depend on the field. In the weak-field limit, the SS energy $E_0(t_i)$ in Eq. (42b) can be approximated by the energy E_0 of the unperturbed initial state, the factor $|A_0(t_i)|^2$ can be expressed in terms of the ionization rate using Eq. (13), and the rate $\Gamma_0(t)$ as a function of the instantaneous field $F(t)$ can be evaluated using the weak-field asymptotic theory [31]. By strong-field effects here we mean departures from these approximations.

The dependence of the quantum shift (42b) on the field is important; however, this effect is small since the shift itself is small, so we do not discuss it here. The weak-field approximation for the rate in the present case of spherically symmetric potentials was obtained in Ref. [43]. This approximation works well only in the deep tunneling regime. It grossly overestimates the ionization rate even for fields in the tunneling

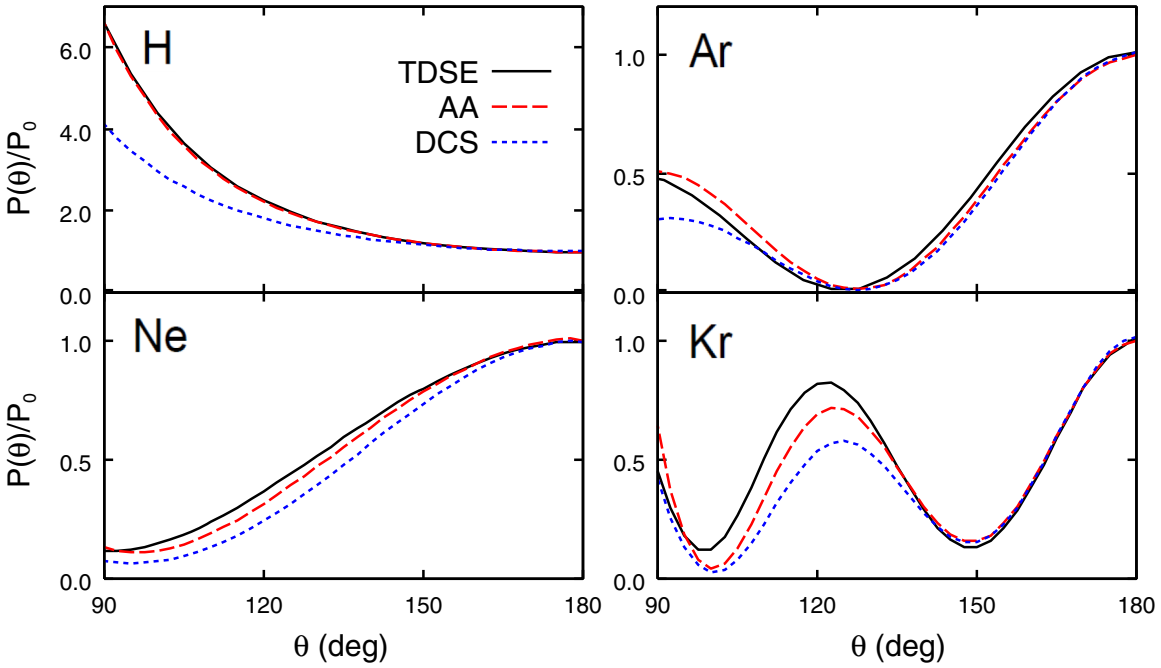

FIG. 8. Cuts of the PEMDs for H($1s$) and noble gas atoms Ne($2p$), Ar($3p$), and Kr($4p$) described by potentials defined in Ref. [42] as functions of θ along the BRC, as in the bottom rows in Figs. 6 and 7. The PEMDs are generated by pulses with $F_0 = 0.08$ and $T = 220$ for H, $F_0 = 0.17$ and $T = 160$ for Ne, $F_0 = 0.1$ and $T = 220$ for Ar, and $F_0 = 0.08$ and $T = 300$ for Kr. The solid (black) lines show cuts $P(\theta)$ of the TDSE PEMDs. The dashed (red) lines show the cuts $P_c(\theta)$ obtained from Eq. (44). The TDSE and AA results in each panel are divided by the same factor $P_0 = P_c(\theta = 180^\circ)$ giving the corresponding value of the AA cut. The dotted (blue) lines show the DCSs as functions of θ at a constant incident momentum $|u_f(180^\circ)|$. The DCS in each panel is multiplied by a factor which brings its value at $\theta = 180^\circ$ in coincidence with the TDSE curve.

regime considered above, let alone for over-the-barrier fields. For example, it overestimates the ionization rate of Xe($5p$) at $F = 0.06$, which corresponds to the pulse amplitude in Fig. 6, by more than a factor of 3 [42]. The error in the ionization rate would be amplified by the exponential function in the depletion factor in Eq. (45). Thus, the strong-field effects in the depletion factor are extremely important: only using accurate ionization rates calculated by the method developed in Ref. [28] were we able to achieve the level of agreement between the TDSE and AA results demonstrated above. This issue is rather trivial, so we do not discuss it further here.

But, the issue related to Eq. (13) is less trivial and deserves an illustration. One could intuitively expect that the ionization step in Eq. (45) should be described by the instantaneous ionization rate $\Gamma_0(t_i)$ instead of the factor $|A_0(t_i)|^2$. This is indeed the case, e.g., in the theory presented in Ref. [8]. In the adiabatic theory, this is the case only in the weak-field limit, when Eq. (13) holds. For stronger fields, even in the tunneling regime and more so in the over-the-barrier regime, the left- and right-hand sides of Eq. (13) differ, and the difference generally grows with the field. This is illustrated in Fig. 9. The RWP (45) is defined by the TMD amplitude taken at zero transverse momentum [see Eq. (12)], and this is also intuitively clear because only electrons released with zero transverse momentum can return for rescattering (see the discussion in Sec. II C). Only in the weak-field limit this amplitude becomes related to the ionization rate via Eq. (13). As seen from Fig. 9, the difference between the left- and right-hand sides of Eq. (13) in the interval of fields considered is rather large. For example, for H($1s$) at $F = 0.08$, which corresponds to the field amplitude for H in Fig. 8, the difference is 13%, while the difference between the AA and TDSE results in the figure is within 2%. Without accounting for this difference, we would not be able to obtain the agreement between the

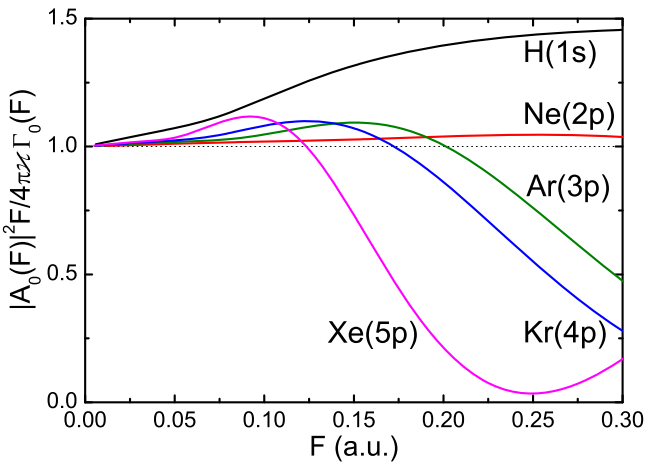

FIG. 9. Ratio of the left-hand side to the right-hand side of Eq. (13) as a function of $F = |F(t)|$ calculated for the $1s$ state of hydrogen and the highest occupied orbital in noble gas atoms described in the single-active-electron approximation using potentials from Ref. [42]. For $F \to 0$, the ratio in all the cases approaches unity, in agreement with Eq. (13).

AA and TDSE results demonstrated above, especially for over-the-barrier fields in Figs. 3, 5, and 7.

IV. CONCLUSIONS

In this paper, the factorization formula (44) describing strong-field photoelectron momentum distributions near the outermost backward rescattering caustic, which was originally inferred on physical grounds in Ref. [3], is derived from the adiabatic theory [26]. The formula accounts for a quantum shift of the caustic and strong-field effects in the returning photoelectron wave packet (45) not discussed previously. The formula is validated by calculations. It is shown to work quantitatively in the vicinity of the caustic in both tunneling and over-the-barrier regimes of ionization for finite-range as well as Coulomb-tail potentials and to become more accurate as the adiabatic parameter giving the ratio of the target and laser field time scales tends to zero. The explicit analytical form of the returning wave packet (45) enables one to extract DCSs for elastic scattering of a photoelectron on the parent ion from experimental photoelectron momentum distributions. The present theory in combination with the experimental technique based on the use of few-cycle pulses with carrier-envelope phase control demonstrated in Ref. [25] establish a quantitative method of extracting the dependence of DCSs on both the incident momentum and the scattering angle.

ACKNOWLEDGMENTS

This work was supported in part by Japan Society for the Promotion of Science KAKENHI Grants No. 16H04029, No. 16H04103, and No. 17K05597. O.I.T. acknowledges support from the Ministry of Education and Science of Russia (State Assignment No. 3.873.2017/4.6) and the Russian Foundation for Basic Research (Grant No. 17-02-00198).

[1] F. Krausz and M. Ivanov, Attosecond physics, Rev. Mod. Phys. **81**, 163 (2009).

[2] G. G. Paulus, W. Becker, W. Nicklich, and H. Walther, Rescattering effects in above-threshold ionization: A classical model, J. Phys. B: At., Mol. Opt. Phys. **27**, L703 (1994).

[3] T. Morishita, A.-T. Le, Z. Chen, and C. D. Lin, Accurate Retrieval of Structural Information from Laser-Induced Photoelectron and High-Order Harmonic Spectra by Few-Cycle Laser Pulses, Phys. Rev. Lett. **100**, 013903 (2008).

[4] Z. Chen, A.-T. Le, T. Morishita, and C. D. Lin, Quantitative rescattering theory for laser-induced high-energy plateau photoelectron spectra, Phys. Rev. A **79**, 033409 (2009).

[5] A. Čerkić, E. Hasović, D. B. Milošević, and W. Becker, High-order above-threshold ionization beyond the first-order Born approximation, Phys. Rev. A **79**, 033413 (2009).

[6] D. B. Milošević, A. Čerkić, B. Fetić, E. Hasović, and W. Becker, Low-frequency approximation for high-order above-threshold ionization, Laser Phys. **20**, 573 (2010).

[7] M. V. Frolov, N. L. Manakov, and A. F. Starace, Analytic formulas for above-threshold ionization or detachment plateau spectra, Phys. Rev. A **79**, 033406 (2009).

[8] M. V. Frolov, D. V. Knyazeva, N. L. Manakov, A. M. Popov, O. V. Tikhonova, E. A. Volkova, M.-H. Xu, L.-Y. Peng, L.-W. Pi, and A. F. Starace, Validity of Factorization of the High-Energy Photoelectron Yield in Above-Threshold Ionization of an Atom by a Short Laser Pulse, Phys. Rev. Lett. **108**, 213002 (2012).

[9] M. V. Frolov, D. V. Knyazeva, N. L. Manakov, J.-W. Geng, L.-Y. Peng, and A. F. Starace, Analytic model for the description of above-threshold ionization by an intense short laser pulse, Phys. Rev. A **89**, 063419 (2014).

[10] O. I. Tolstikhin, T. Morishita, and S. Watanabe, Adiabatic theory of ionization of atoms by intense laser pulses: One-dimensional zero-range-potential model, Phys. Rev. A **81**, 033415 (2010).

[11] M. Okunishi, T. Morishita, G. Prümper, K. Shimada, C. D. Lin, S. Watanabe, and K. Ueda, Experimental Retrieval of Target Structure Information from Laser-Induced Rescattered Photoelectron Momentum Distributions, Phys. Rev. Lett. **100**, 143001 (2008).

[12] D. Ray, B. Ulrich, I. Bocharova, C. Maharjan, P. Ranitovic, B. Gramkow, M. Magrakvelidze, S. De, I. V. Litvinyuk, A.-T. Le *et al.*, Large-Angle Electron Diffraction Structure in Laser-Induced Rescattering from Rare Gases, Phys. Rev. Lett. **100**, 143002 (2008).

[13] T. Morishita, M. Okunishi, K. Shimada, G. Prümper, K. Shimada, Z. Chen, S. Watanabe, K. Ueda, and C. D. Lin, Retrieval of experimental differential electron-ion elastic scattering cross sections from high-energy ATI spectra of rare gas atoms by infrared lasers, J. Phys. B: At., Mol. Opt. Phys. **42**, 105205 (2009).

[14] C. Cornaggia, Electron-ion elastic scattering in molecules probed by laser-induced ionization, J. Phys. B: At., Mol. Opt. Phys. **42**, 161002 (2009).

[15] M. Okunishi, H. Niikura, R. R. Lucchese, T. Morishita, and K. Ueda, Extracting Electron-Ion Differential Scattering Cross Sections for Partially Aligned Molecules by Laser-Induced Rescattering Photoelectron Spectroscopy, Phys. Rev. Lett. **106**, 063001 (2011).

[16] C. Wang, M. Okunishi, R. R. Lucchese, T. Morishita, O. I. Tolstikhin, L. B. Madsen, K. Shimada, D. Ding, and K. Ueda, J. Phys. B: At., Mol. Opt. Phys. **45**, 131001 (2012).

[17] M. Okunishi, R. R. Lucchese, T. Morishita, and K. Ueda, Rescattering photoelectron spectroscopy of small molecules, J. Electron Spectrosc. Relat. Phenom. **195**, 313 (2014).

[18] T. Morishita, T. Umegaki, S. Watanabe, and C. D. Lin, High-resolution spatial and temporal microscopy with intense-laser-induced rescattering electrons, J. Phys.: Conf. Ser. **194**, 012011 (2009).

[19] J. Xu, C. I. Blaga, A. D. DiChiara, E. Sistrunk, K. Zhang, Z. Chen, A.-T. Le, T. Morishita, C. D. Lin, P. Agostini, and L. F. DiMauro, Laser-Induced Electron Diffraction for Probing Rare Gas Atoms, Phys. Rev. Lett. **109**, 233002 (2012).

[20] C. I. Blaga, J. Xu, A. D. DiChiara, E. Sistrunk, K. Zhang, P. Agostini, T. A. Miller, L. F. DiMauro, and C. D. Lin, Imaging ultrafast molecular dynamics with laser-induced electron diffraction, Nature (London) **483**, 194 (2012).

[21] J. Xu, C. I. Blaga, K. Zhang, Y. H. Lai, C. D. Lin, T. A. Miller, P. Agostini, and L. F. DiMauro, Diffraction using laser-driven broadband electron wave packets, Nat. Commun. **5**, 4635 (2014).

[22] M. Pullen, B. Wolter, A.-T. Le, M. Baudisch, M. Hemmer, A. Senftleben, C. D. Schröter, J. Ullrich, R. Moshammer, C. D. Lin, and J. Biegert, Imaging an aligned polyatomic molecule with laser-induced electron diffraction, Nat. Commun. **6**, 7262 (2015).

[23] B. Wolter, M. G. Pullen, A.-T. Le, M. Baudisch, K. Doblhoff-Dier, A. Senftleben, M. Hemmer, C. D. Schröter, J. Ullrich, T. Pfeifer *et al.*, Ultrafast electron diffraction imaging of bond breaking in di-ionized acetylene, Science **354**, 308 (2016).

[24] Y. Ito, C. Wang, A.-T. Le, M. Okunishi, D. Ding, C. D. Lin, and K. Ueda, Extracting conformational structure information of benzene molecules via laser-induced electron diffraction, Struct. Dynamics **3**, 034303 (2016).

[25] H. Geiseler, N. Ishii, K. Kaneshima, F. Geier, T. Kanai, O. I. Tolstikhin, T. Morishita, and J. Itatani, Carrier-envelope phase mapping in laser-induced electron diffraction, Phys. Rev. A **94**, 033417 (2016).

[26] O. I. Tolstikhin and T. Morishita, Adiabatic theory of ionization by intense laser pulses: Finite-range potentials, Phys. Rev. A **86**, 043417 (2012).

[27] R. G. Newton, *Scattering Theory of Waves and Particles* (Springer, New York, 1982).

[28] P. A. Batishchev, O. I. Tolstikhin, and T. Morishita, Atomic Siegert states in an electric field: Transverse momentum distribution of the ionized electrons, Phys. Rev. A **82**, 023416 (2010).

[29] L. Hamonou, T. Morishita, and O. I. Tolstikhin, Molecular Siegert states in an electric field, Phys. Rev. A **86**, 013412 (2012).

[30] V. N. T. Pham, O. I. Tolstikhin, and T. Morishita, Molecular Siegert states in an electric field. II. Transverse momentum distribution of the ionized electrons, Phys. Rev. A **89**, 033426 (2014).

[31] O. I. Tolstikhin, T. Morishita, and L. B. Madsen, Theory of tunneling ionization of molecules: Weak-field asymptotics including dipole effects, Phys. Rev. A **84**, 053423 (2011).

[32] M. Spanner, O. Smirnova, P. B. Corkum, and M. Yu. Ivanov, Reading diffraction images in strong field ionization of diatomic molecules, J. Phys. B: At., Mol. Opt. Phys. **37**, L243 (2004).

[33] *Handbook of Mathematical Functions*, edited by M. Abramowitz and I. A. Stegun (Dover, New York, 1972).

[34] M. Busuladžić, A. Gazibegović-Busuladžić, and D. B. Milošević, High-order above-threshold ionization in a laser field: Influence of the ionization potential on the high-energy cutoff, Laser Phys. **16**, 289 (2006).

[35] C. Chester, B. Friedman, and F. Ursell, An extension of the method of steepest descents, Math. Proc. Cambridge Philos. Soc. **53**, 599 (1957).

[36] L. D. Landau and E. M. Lifshitz, *The Classical Theory of Fields* (Butterworth-Heinemann, Oxford, 1980).

[37] A. I. Nikishov and V. I. Ritus, Quantum Processes in the Field of a Plane Electromagnetic Wave and in a Constant Field. I, Zh. Eksp. Teor. Fiz. **46**, 776 (1964) [Sov. Phys.–JETP **19**, 529 (1964)].

[38] M. Lewenstein, Ph. Balcou, M. Yu. Ivanov, A. LHuillier, and P. B. Corkum, Theory of high-harmonic generation by low-frequency laser fields, Phys. Rev. A **49**, 2117 (1994).

[39] O. Smirnova and M. Ivanov, Multielectron High Harmonic Generation: Simple Man on a Complex Plane, in *Attosecond and XUV Physics: Ultrafast Dynamics and Spectroscopy*, edited by T. Schultz and M. Vrakking (Wiley, Weinheim, 2014), Chap. 7.

[40] S. P. Goreslavskii and S. V. Popruzhenko, Simple quantum theory of the high-energy above-threshold ionization spectrum in the tunneling regime, Phys. Lett. A **249**, 477 (1998).

[41] T. Morishita, Z. Chen, S. Watanabe, and C. D. Lin, Two-dimensional electron momentum spectra of argon ionized by short intense lasers: Comparison of theory with experiment, Phys. Rev. A **75**, 023407 (2007).

[42] V. H. Trinh, O. I. Tolstikhin, L. B. Madsen, and T. Morishita, First-order correction terms in the weak-field asymptotic theory of tunneling ionization, Phys. Rev. A **87**, 043426 (2013).

[43] B. M. Smirnov and M. I. Chibisov, The breaking up of atomic particles by an electric field and by electron collisions, Zh. Eksp. Teor. Fiz. **49**, 841 (1965) [Sov. Phys.–JETP **22**, 585 (1966)].